HHS Public Access

Author manuscript

*Nat Med*. Author manuscript; available in PMC 2016 April 01.

Published in final edited form as:

*Nat Med*. 2015 October ; 21(10): 1223–1227. doi:10.1038/nm.3937.

# The association between sterilizing activity and drug distribution into tuberculosis lesions

**Brendan Prideaux**[1], **Laura E. Via**[2], **Matthew D. Zimmerman**[1], **Seokyong Eum**[3], **Jansy Sarathy**[1], **Paul O'Brien**[1], **Chao Chen**[1], **Firat Kaya**[1], **Danielle M. Weiner**[2], **Pei-Yu Chen**[1], **Taeksun Song**[3], **Myungsun Lee**[3], **TaeSun Shim**[4], **Jeong Su Cho**[5], **Wooshik Kim**[6], **Sang Nae Cho**[7], **Kenneth N. Olivier**[8], **Clifton E. Barry III**[2,9,*], and **Véronique Dartois**[1,*]

[1]Public Health Research Institute, New Jersey Medical School, Rutgers, The State University of New Jersey

[2]Tuberculosis Research Section, Laboratory of Clinical Infectious Diseases, National Institute of Allergy and Infectious Diseases, National Institutes of Health, Bethesda, MD, USA

[3]International Tuberculosis Research Center, Changwon, Republic of Korea

[4]Asan Medical Center, Seoul, Republic of Korea

[5]Pusan National University Hospital, Pusan, Republic of Korea

[6]National Medical Center, Seoul, Republic of Korea

[7]Department of Microbiology and Institute of Immunology and Immunological Disease, Yonsei University College of Medicine, Seoul, Republic of Korea

[8]Pulmonary Clinical Medicine, Cardiovascular Pulmonary Branch, National Hearth Lung Blood Institute, National Institutes of Health, Bethesda, MD, USA

[9]Institute of Infectious Disease and Molecular Medicine, Department of Clinical Laboratory Sciences, University of Cape Town, Cape Town, South Africa

## Abstract

Finding new treatment-shortening antibiotics to improve cure rates and curb the alarming emergence of drug resistance is the major objective of tuberculosis (TB) drug development. Using a MALDI mass spectrometry imaging suite in a biosafety containment facility, we show that the key sterilizing drugs rifampicin and pyrazinamide efficiently penetrate the sites of TB infection in lung lesions. Rifampicin even accumulates in necrotic caseum, a critical lesion site where



*Correspondence to: cbarry@niaid.nih.gov and veronique.dartois@rutgers.edu.

**Author Contributions:** B.P. and P.-Y.C. developed all MALDI MSI methods and imaged the study drugs in lung biopsies; L.E.V., C.E.B., S.N.C. and V.D. conceived the study and wrote the clinical protocol; L.E.V. and S.E. developed the dissection protocol and conducted lung dissections; M.D.Z. and F.K. quantified all study drugs in plasma, lung and lesions; J.S., P.O.B., D.M.W. and F.K. developed methods to sterilize TB-infected samples and extract the study drugs; J.S. and C.C. developed the caseum binding and macrophage uptake assay and quantified the study drugs; T.S. collated clinical and radiological data and facilitated sample collection and transport; M.L. coordinated patient enrollment, confirmed study eligibility and facilitated case reporting; T.S.S., J.S.C., W.K., S.N.C. and K.N.O. coordinated lung resection surgeries; C.E.B. and V.D. wrote the manuscript.

The authors declare no competing financial interests

persisting tubercle bacilli reside[1]. In contrast, moxifloxacin which is active *in vitro* against persisters, a sub-population of *Mycobacterium tuberculosis* that persists in specific niches under drug pressure, and achieved treatment shortening in mice[2], does not diffuse well in caseum, concordant with its failure to shorten therapy in recent clinical trials. We also suggest that such differential spatial distribution and kinetics of accumulation in lesions may create temporal and spatial windows of monotherapy in specific niches, allowing the gradual development of multidrug resistant TB. We propose an alternative working model to prioritize new antibiotic regimens based on quantitative and spatial distribution of TB drugs in the major lesion types found in human lungs. The finding that lesion penetration contributes to treatment outcome has wide implications for TB.

## INTRODUCTION

Standard treatment of drug susceptible tuberculosis requires six months of combination therapy including three key drugs: isoniazid (INH), rifampicin (RIF) and pyrazinamide (PZA). This regimen was named “short course” therapy because it provided, at the time of its introduction, a dramatic shortening of the previous two-year treatment[3]. Reduced chemotherapy duration was achieved by the introduction of RIF and PZA, which are called ‘sterilizing’ drugs as they clear difficult-to-eradicate forms of the pathogen[4]. The main objective of contemporary TB drug development remains shortening curative treatment duration, in hopes of reducing non-adherence and the emergence of genetically drug resistant *Mycobacterium tuberculosis* which present major challenges in global TB control. Here we use MALDI imaging mass spectrometry to show that the patterns of drug penetration provide a critical insight into the ability of individual drugs to sterilize lesion compartments where persisting bacteria have been shown to reside[1,5]. Such distinct patterns of drug partitioning may generate temporal and spatial windows of monotherapy, with the potential for emergence of genetic drug resistance. This approach may help guide the rational selection of new drug regimens for clinical development to improve the odds of success in future trials.

Historically, the contribution of each drug in the standard regimen to durable cure has been explained by the unique metabolic characteristics of *M. tuberculosis* subpopulations associated with lesion-specific microenvironments[4]. It is believed that, in aerobic microenvironments with neutral pH, the bacilli are metabolically active and susceptible to killing by INH and RIF. In contrast, anaerobic microenvironments slow the growth of the obligate aerobic bacillus, which then become tolerant to the cell wall synthesis inhibitor INH while remaining susceptible to the RNA polymerase inhibitor RIF. Other specialized microenvironments such as the phagolysosome of infected macrophages are thought to be acidic, resulting in slow growing bacilli that are specifically susceptible to PZA, which is only active at acidic pH. In this scenario, RIF and PZA would be sterilizing because they are uniquely capable of killing metabolically adapted, drug-tolerant ‘persister’ populations. The gyrase inhibitor moxifloxacin (MXF), which was recently tested in clinical trials for shortening front line treatment, kills growing as well as anaerobic non-replicating bacteria *in vitro*[6], similar to RIF. MXF was therefore expected to exhibit ‘sterilizing’ activity *in vivo*, and mouse efficacy trials further supported this expectation[7]. However, two large Phase III

trials have failed to confirm the pre-clinical results and showed no shortening of duration of treatment[8,9] In the wake of these failures, we have considered an alternative working model to predict sterilizing activity based on quantitative and spatial distribution of TB drugs in the major lesion types found in human lungs[10].

## RESULTS and DISCUSSION

We recruited a cohort of 15 TB-infected participants who were scheduled to undergo lung resection surgery for drug-refractory disease (Table S1). All 15 subjects received a single dose of a cocktail containing INH, RIF, PZA and MXF at pre-specified times prior to surgery. The times of drug administration were randomly assigned to five groups of three subjects, from 2 to 24 h pre-surgery (Fig.S1). Upon lung resection, an average of 12 discrete lesions per subject were dissected and processed for histopathology, determination of drug concentration, and imaging mass spectrometry. Dissected tissues were classified as uninvolved lung, closed nodules (either cellular, necrotic and/or fibrotic), cavity wall, cavity caseum, or nodule caseum. Lesion weight and size were recorded. We measured the absolute drug concentrations of INH, RIF, PZA and MXF in plasma (Fig.S2), lung (Fig. S3) and lesions over the 24h dosing interval, as well as their major metabolites: inactive acetyl-INH, desacetyl-RIF one-third as potent as RIF, and active POA which is produced both by the host and the pathogen[11]. Fig.1 shows the concentrations of drugs and metabolites in homogenized lesions, relative to the aerobic minimum inhibitory concentration (MIC) and the minimum anaerobic cidal concentration (MAC), a measure of drug activity against bacilli persisting in necrotic lesions where anaerobic conditions prevail[12]. The MAC values are averages obtained using laboratory strains and may not capture population-specific variability. INH concentrations were above the MIC in most lesions (65%) but never reached the MAC since the drug lacks activity against non-replicating anaerobic bacilli (Fig. 1a). RIF concentrations were above the MIC range in almost all lesions, and at or above the MAC in 64% of the lesions (Fig.1b). The levels of PZA, a drug that inhibits growth only at acidic pH *in vitro*[13], were within its ‘acidic’ MIC range (Fig.1c). Pyrazinoic acid, an active metabolite of PZA, distributed into all lesions types to the same extent as PZA (Fig.S4). MXF, unlike INH, RIF and PZA, was consistently present at significantly higher concentrations in lesions than in plasma (Fig.S6b–e). MXF levels were above the MIC in all lesion homogenates, and at or above the MAC in 38% of the lesions (Fig.1D), indicating that it might reach non-growing persisters at therapeutic concentrations.

In lesion homogenates, absolute drug concentrations are a useful measure of exposure at the site of infection, but important information on the spatial distribution of drugs in distinct compartments is lost. The spectrum of TB lesions is diverse: cellular granulomas consisting of a rim of lymphocytes surrounding neutrophils and macrophages, caseous granulomas in which necrosis or apoptosis of infected cells generates a mass of cellular debris devoid of blood supply, and cavities resulting from the destructive erosion of lesions into major airways[14]. Mature lesions are encapsulated within layers of fibroblasts, which further serves to wall off the infection. The presence and extent of cavitary disease are correlates of poor clinical outcome and relapse[15,16]. To study the spatial distribution of TB drugs in intact lesions, we used a MALDI mass spectrometry suite[17,18] inside a biosafety level three high containment facility, allowing imaging of unlabeled drug molecules in human lesions (Fig.

2a and S3). High resolution (30–100 μm) images of RIF, PZA, MXF and acetyl-INH (used as a surrogate of INH based on similar distribution into lesions [Fig.1]) in necrotic granulomas were obtained from biopsies collected between 3 and 25 h post drug administration, and superimposed onto histological staining of adjacent sections, revealing lesion structure. These maps demonstrated differential penetration of each drug or metabolite in caseous foci versus cellular layers. PZA (Fig.2b, S4) and AcINH (Fig.S5) diffused favorably and rapidly into the necrotic cores and subtending cellular layers where persister bacilli are found in the acidic phagolysosome of macrophages[19]. Thus, PZA's sterilizing activity could result from equally rapid and effective distribution in the caseum and the cellular region of granulomas, where it reaches and kills both extracellular and intra-phagosomal bacterial populations. Overall INH, PZA and its active metabolite POA, small and polar molecules, showed homogeneous distribution across tissue types, with similar concentrations in the cavity wall and caseum of subjects with cavitary disease (Fig.S4). MXF exhibited a very different distribution pattern. Whereas the drug accumulated in cellular regions, it did not diffuse well into acellular caseum (Fig.2b, S4). Relative drug abundance measured in regions of interest of selected ion maps confirmed the visual trend of distribution in cellular rim and caseous foci (Fig. S4f). Upon closer examination of MALDI images and absolute concentrations in lesions, we found that MXF penetration into the caseum of cavities and closed nodules was variable. Histological staining of lesions indicated that caseum presented with a spectrum of 'cellularity', from fully acellular and made exclusively of cellular debris, to caseum made of >50% intact cells. Since MXF is known to accumulate in immune cells *in vitro*, particularly activated macrophages[20], we hypothesized that this variability in caseum partitioning could be associated with the degree of caseum cellularity. Indeed, we found a correlation between caseum cellularity and the extent of MXF partitioning into caseum (Fig.2c)[20]. Thus, failure of MXF to shorten TB treatment in clinical trials[8,9] might be explained by the drug's inability to achieve adequate concentrations in critical niches where the bacilli reside. The MXF distribution patterns observed here agree well with our previous quantitative analysis[21] and imaging[22] of this drug in necrotic rabbit granulomas. Overall, the two-dimensional maps of RIF, PZA, POA and MXF in rabbit lesions (Fig S7) are similar to the corresponding drug maps of human lesions, confirming that the rabbit model is an adequate tool to study lesion pharmacokinetics.

To investigate drug accumulation into tissues at steady-state, we focused on a subset of the subjects who had received daily INH, PZA or MXF as standard of care for several months prior to surgery (Table S1). None of the three drugs accumulated to higher levels in the lesions of these subjects, compared to those who received a single dose (Fig.2, S5, S6), indicating rapid clearance of INH, PZA and MXF from the tissues as observed in plasma (Fig. S2). The three drugs distributed rapidly into lesions as demonstrated by plotting average lesion/plasma ratios over the course of one dosing interval (Fig.S6b–e). In contrast to the cumulative dose-independent distribution of INH, PZA and MXF, RIF (and desacetyl-RIF) accumulated in caseum after multiple doses (Fig. 3ab, S4f and S8), and remained present at easily detectable levels in the necrotic lesions after falling below the limit of detection in uninvolved lung and plasma (Fig.3bc). Thus, while the caseum/cellular concentration ratio of MXF is <1 and independent of the number of doses received, RIF

accumulates in necrotic foci to reach caseum/cellular ratios >10, more than 20-fold higher at steady state than after a single dose (the former being clinically more relevant). This sustained accumulation in the necrotic core of nodules and cavities, combined with the unique potency of RIF against non-replicating bacilli[4,6], may explain RIF's excellent sterilizing activity in patients.

We next applied our lesion penetration approach to clofazimine (CFZ), a leprosy drug currently currently in clinical trials for use in TB. CFZ proved very efficacious in BALB/c mice where granulomas are exclusively cellular, but displayed minimal activity in C3HeB/FeJ mice which develop large necrotic lesions with high bacillary burden[23,24]. We quantified and imaged the distribution of CFZ in three subjects (two of which were part of the cohort of 15, while the third one did not receive the four study drugs) who had received the drug as part of their prescribed regimen for several months. CFZ showed a contrasting partitioning between the cellular rim and necrotic core of lesions, with strong accumulation in cellular layers relative to caseum (Fig.S9a). CFZ quantification in plasma, cavity wall and cavity caseum clearly confirmed the imaging results (Fig. S8b). Thus, the lack of CFZ diffusion into necrotic foci may contribute to its limited activity in C3HeB/FeJ, a finding which should be considered when selecting drug regimens for future clinical trials.

What mechanisms drive the distribution of drugs into avascular caseum? We reasoned that drug molecules present in the interstitial fluid at the interface between the cellular rim and the necrotic core can be subjected to: (1) active transport into macrophages and other immune cells[25], (2) binding to extracellular macromolecules/proteins, (3) free diffusion through non-vascularized caseum. To understand drug partitioning at the cellular-necrotic interface, we measured the intra-macrophage uptake and *ex vivo* caseum binding of RIF, Acetyl-INH, PZA, MXF and CFZ. We observed a wide range of intracellular uptake into macrophages, in agreement with literature data for CFZ and MXF[20,26]. As ClogP (octanol:water partitioning) and thus hydrophobicity increases, non-specific protein binding increases, with two important implications: the free fraction available to passively diffuse through caseum decreases, and intracellular accumulation in macrophages increases due to uptake of protein:drug complexes by endocytosis and lysosomal trapping (among other mechanisms). Less lipophilic drugs may also dissolve in interstitial fluid and from there gradually accumulate inside the caseum. Under this model, favorable diffusion through caseum is the result of a delicate balance between active transport, protein binding and physico-chemical properties driving solubility and diffusion ability'. Rifampicin may lie in the 'sweet spot' by combining relatively low uptake into macrophages, and ideal caseum binding leading to sustained accumulation into necrotic cores (Fig.4 and S10).

We have demonstrated that different drugs exhibit different spatial and temporal patterns of distribution across TB lesion types and compartments. The results provide a spatial pharmacokinetic and pharmacodynamics explanation for the treatment shortening properties (or lack thereof) of current TB drugs. Favorable penetration alone is not sufficient, neither is activity, as exemplified by INH and MXF, respectively. The key sterilizing drugs RIF and PZA achieve adequate concentrations in critical lesion compartments. PZA distributed equally well in caseous and cellular compartments, thus reaching two critical persister populations: extracellular anaerobic bacilli in caseum and intracellular bacteria in acidic

phagolysosomes[27]. RIF showed sustained accumulation over time in necrotic caseum where extracellular anaerobic bacteria reside. MXF did not reach concentrations required to kill non-replicating bacteria in the caseum of cavities and nodules, a potential explanation for its performance in recent trials. Such differential drug distribution and kinetics of accumulation in lesions may create temporal and spatial windows of monotherapy in specific niches, allowing the multiplication of single drug resistant mutants and the gradual development of multidrug resistant TB. The stepwise development of drug resistance has been demonstrated in individual patients using conventional typing methods[28] or whole genome sequencing more recently[29]. Deep lesion sequencing has revealed complex intra-patient microevolution of *M. tuberculosis* leading to diverging clonal populations with distinct resistance patterns[30,31]. The selection of new drug combinations should be supported by lesion penetration data in animal models with caseous lesions to ensure multidrug coverage in a given lesion compartment and limit the occurrence of de facto monotherapy. Our results suggest that persistent pathology may be as important for determining sterilizing activity as persistent organisms, and pave the way for a more rational approach that combines agents which together reach all target bacterial populations at therapeutic concentrations, a significant departure from the current – and mostly empirical – paradigm. Such a strategy is expected to reduce costly attrition in late phase clinical development, an important consideration for a disease that largely affects resource-limited populations.

## METHODS

### Clinical research study design and institutional approvals

Adults with pulmonary MDR-TB scheduled for elective lung resection surgery were asked to participate in the study “Pharmacokinetics of Standard First and Second Line anti-TB Drugs in the Lung and Lesions of Subjects Elected for Resection Surgery” (www.ClinicalTrials.gov#NCT00816426). The institutional review boards of the National Institute of Allergy and Infection Disease, National Institutes of Health, Bethesda, Maryland USA and the hospitals Pusan National University Hospital, Pusan, Republic of Korea (ROK); Asan Medical Center, Seoul, ROK; and National Medical Center, Seoul, ROK all approved the study. The procedures followed were in accordance with the ethical standards of the Helsinki Declaration. Of the nineteen subjects who gave consent for the study, three were found to be ineligible due to underlying conditions or the investigator’s decision and one withdrew consent. Fifteen consented subjects were randomized to receive three first-line and two second-line anti-TB agents as follows: 600mg RIF (450mg for patients less than 50kg in body weight), 300mg INH, 1500mg PZA, and 400mg MXF administered orally (i.e. all 15 subjects received the 4 study drugs). All 5 anti-TB drugs were administered concomitantly at 2, 4, 8, 12 or 24h prior to scheduled surgery, with 3 subjects randomized to each of the 5 target timepoints. Subjects were assigned to one of the 5 drug administration times by simple randomization. A single balanced list of ID numbers with the 5 drug dose times permuted randomly across the IDs was provided by the statistician to the centralized monitoring organization who managed the randomization assignments for the 3 clinical sites. Each time a subject was consented and enrolled, a designee at that site contacted the monitoring organization who assigned the next study ID and drug dosing time on the list.

All subjects had been treated for TB prior to the study, and had thus received a specific drug regimen tailored to their respective drug susceptibility profile. Thus, a subset of the subjects had received either INH, PZA or MXF as part of their background drug regimen for several weeks or months prior to surgery (see Table S1 for a complete list of background drugs) and were at steady-state for these drugs. Two subjects had received CFZ as part of their standard-of-care. During the surgery, the exact time of pulmonary artery ligation was recorded and used to back calculate the time of drug administration relative to surgery. Actual times of drug administration varied from 3.3 to 25h prior to pulmonary vessel ligation. Three surgeries took longer than anticipated, with the target timepoint post drug administration being longer than the target window (by 1h to 4h30). This did not affect the dataset since the actual time lapse from drug administration to termination of tissue blood flow was used in each participant's case.

One adult with chronic *Mycobacterium abscessus* infection scheduled for elective surgery at the NIH Clinical Centre gave written consent to participate under NIAID study "Study of Mycobacterial Infections" (www.ClinicalTrials.gov#NCT00018044). This participant had pulmonary nontuberculous mycobacterial disease presenting with cavitary lesions, well-organized necrotizing granulomas, and non-necrotizing granulomas similar to those described previously in lung disease caused by non-TB mycobacteria and *M. tuberculosis*[33–35]. This 73 year-old female participant was administered 600mg RIF and 100mg CFZ daily among other anti-mycobacterial medications as part of her standard drug regimen (24h target group, 26h (for RIF) and 27h (for CFZ) actual times of vessel ligation post drug administration). This individual was at steady-state for both RIF and CFZ.

All participants had at least one prior episode of anti-TB or anti-mycobacterial treatment (median episodes 1, range 1 to 8). The median age was 45 (range 23 to 59), nine were male and all were Asian. The weight range was 49.8 to 84.0 kg, with a median of 57.8kg. Mean weights (± SD) were 65 ± 12 kg and 53 ± 3 kg for males and females, respectively. Table S2 summarizes subjects' demographics. Subjects were followed for one month post-surgery for drug related adverse effects.

### Sample size justification

The sample size for this study was determined based on the number of subjects necessary to detect a 50% difference in the permeability coefficient into caseous necrotic nodules between 2 different drugs with 80% power. Comparison of the permeability coefficient was chosen as the primary endpoint rather than drug exposure in lesions relative to plasma. This type of endpoint is often adopted in case of sparse PK sampling design, where each subject contributes plasma and tissue PK measurements at one or few time points. In such case, AUC or drug exposure over time cannot be estimated accurately but is rather fit to a model. On the other hand, since each time point/subject was expected to contribute serial plasma, lung tissue and at least 2–5 lesion measurements (largely exceeded in this study), an estimation of P for each drug, using pooled PK data across subjects, can be made with much better precision than an estimation of AUC. The variability of the permeability coefficient (P) across subjects or between similar lesions within one subject was expected to be around 50%, based on permeability coefficients in abscesses[36]. With these assumptions, and

normally distributed differences in the coefficient P between 2 drugs, a paired t-test would have required 12 subjects. A 20% inflation factor was applied to the sample size to allow for loss of data due to some administrative or analytical issues. The required sample size for this study is thus 15 subjects. The total number of lesions sampled was 173 across 15 subjects, thus 11.6 lesions per subject. All lesion samples contained the 4 study drugs. Exclusion criteria were as follows:

1. Subjects <20 years of age
2. Women of childbearing potential, who are pregnant, breast feeding, or unwilling to avoid pregnancy (i.e., the use of appropriate contraception including oral and subcutaneous implantable hormonal contraceptives, condoms, diaphragm, intrauterine device (IUD), or abstinence from sexual intercourse) [Note: Prospective female participants of childbearing potential must have negative pregnancy test (urine) within 48 hours prior to study entry.]
3. Allergy or hypersensitivity to any of the 5 study drugs or any fluoroquinolone, aminoglycoside, or rifamycin
4. Those with severe gout
5. Severe claustrophobia or Gadolinium hypersensitivity (tbc)
6. Renal, hepatic, auditory and/or vestibular impairment.
    a. Serum creatinine >2.0 mg/dL (renal)
    b. Aspartate aminotransferase (AST or SGOT) >100 IU/L (LFTs)
    c. Alanine aminotransferase (ALT or SGPT) >100 IU/L (LFTs)
    d. Total bilirubin >2.0 mg/dL (LFTs)
7. Documented QT prolongation
8. The use of any of Rifampicin (RIF), Rifapentine or Rifabutin within 30 days prior to the study
9. HIV infection, determined by a positive HIV test performed with the past 6 months
10. The use of any of the following drugs within 30 days prior to study
    a. Systemic cancer chemotherapy
    b. Chronic systemic corticosteroids (oral or IV only) with the following exceptions (i.e., the following are NOT exclusion criteria): intranasal, topical, and inhaled corticosteroids, a short course (10 days or less) of corticosteroids for a non-chronic condition completed at least 2 weeks prior to enrollment in this study
    c. Systemic IND agents other than linezolid
    d. Antiretroviral medications
    e. Growth factors

11. The need for ongoing therapy with warfarin, phenytoin, lithium, cholestyramine, levodopa, cimetidine, disulfiram, ergot derivatives, fosphenytoin, carbamazepine, cyclosporine, tacrolimus, sirolimus, amiodarone or phenobarbital (If a potential subject is on one of these medications but it is being stopped per standard of care, to be eligible for the study the drug must be stopped at least one day prior to receiving study drug. A longer washout period is not necessary.) The only exception to this is amiodarone; because of amiodarone's long half-life and potential for QT prolongation, it should be stopped at least 60 days prior to receiving study drugs.

## Sample collection and processing

Plasma was collected from each subject pre-dose, at 2h and 6h following administration of the study drugs, at the time of pulmonary artery ligation and of lung resection. There was no blood collected at 6h for the subjects who were randomized to receive the study drugs 2 and 4h prior to surgery.

For each subject, the resected lung tissue was collected in a sterile container by the study nurse from the surgical suite and delivered immediately to the dissection team. The tissue was photographed and palpated to identify the location of the lesions observed in the pre-surgery computed tomographic scan. Apparently non-diseased tissue specimens were removed and frozen in liquid nitrogen first. The lung tissue was then sliced in approximately 0.5 cm slices to reveal the cavities and nodules and other lesions. Each lesion was measured, classified, mapped, and divided into parts for analytical drug quantitation by high pressure liquid chromatography coupled to tandem mass spectrometry (LC/MS-MS), MALDI mass spectrometry imaging (MSI), and histology as described previously[21,22]. For analytical drug measurement, the lesions were carefully dissected away from the surrounding tissue while the portion of the lesion used for MALDI imaging was left embedded in the surrounding tissue. When lesions greater than 4mm had separable necrotic contents, separate samples of the lesion wall and caseous material were stored for determination of drug levels. Lesion samples for histological analysis were placed in neutral buffered formalin overnight, dehydrated and embedded in paraffin by standard methods.

Tissue samples were weighed and homogenized in approximately – but accurately recorded – 5 to 7 volumes of phosphate buffered saline (PBS). Homogenization was achieved using a FastPrep-24 instrument (MP Biomedicals) and 1.4mm zirconium oxide beads (Precellys). Proteins were precipitated by adding 9 volumes of 1:1 acetonitrile:methanol containing 0.5μg/ml of internal standards to 1 volume of plasma or homogenized tissue sample. The mixtures were vortexed for 5min and centrifuged at 4,000rpm for 5min. The supernatant was then transferred for LC/MS-MS analysis. All tissue samples were homogenized and diluted 5-fold in PBS. Homogenization was achieved using a FastPrep-24 instrument (MP Biomedicals) and 1.4mm zirconium oxide beads (Precellys). Proteins were precipitated by adding 180μl of 1:1 acetonitrile:methanol containing relevant internal standards to 20μl of plasma or homogenized tissue sample. The mixtures were vortexed for 5min and centrifuged at 4,000rpm for 5min. The supernatant was then transferred for LC/MS analysis.

## LC/MS-MS analytical methods

LC/MS-MS analysis was performed on a Sciex Applied Biosystems Qtrap 4000 triple-quadrupole mass spectrometer coupled to an Agilent 1260 HPLC system to quantify each drug in the clinical samples. PZA and pyrazinoate chromatography was performed with an Agilent Zorbax SB-C8 column (4.6×75 mm; particle size, 3.5μm) using a reverse phase gradient elution. Cynnamaldehyde-INH derivative, MXF, RIF, Des-RIF, and CFZ chromatography was performed on an Agilent Zorbax SB-C8 column (2.1×30 mm; particle size, 3.5μm) using a reverse phase gradient elution. Ac-INH chromatography was performed on a Cogent Diamond Hydride column (2.1×50 mm; particle size, 4μm) using a normal phase gradient. All gradients used 0.1% formic acid in Milli-Q deionized water for the aqueous mobile phase and 0.1% formic acid in acetonitrile for the organic mobile phase. Multiple-reaction monitoring of parent/daughter transitions in electrospray positive-ionization mode was used to quantify the analytes. Sample analysis was accepted if the concentrations of the quality control samples were within 20% of the nominal concentration. Data processing was performed using Analyst software (version 1.6.2; Applied Biosystems Sciex).

Neat 1mg/mL DMSO stocks for all compounds were serial diluted in 50/50 Acetonitrile water to create standard curves and quality control spiking solutions. 20μLs of neat spiking solutions were added to 20μLs of drug free plasma or control tissue homogenate, and extraction was performed by adding 180 μLs of Acetonitrile/Methanol 50/50 protein precipitation solvent containing the internal standards for all drugs except INH. Extracts were vortexed for 5 minutes and centrifuged at 4000 RPM for 5 minutes. The supernatant was transferred for HPLC-MS/MS analysis. INH extraction was performed by adding 30μL of 35% Trichloroacetic Acid (TCA) in water to study samples to precipitate proteins. Extracts were vortexed for 5 minutes and 80 μL of internal standard solution (INH-D4 in 1% Formic Acid in water) was added to the extract, vortexed again for 5 minutes and centrifuged at 4000 RPM for 5 minutes. The supernatant was transferred to a 96 Well plate and trans-Cinnamaldehyde (50× diluted in Methanol) was added to the extracts 1:1 (v:v) to derivatize INH and INH-D4.

Human control plasma ($K_2$EDTA, Bioreclamation IVT, NY) was used to build standard curves. Gamma irradiated lung, lesion, and caseum from tuberculosis infected New Zealand White rabbits was used as a surrogate matrix for human tissues to build standard curves. Surrogate matrices were homogenized by adding 4 parts PBS buffer: 1 part surrogate tissue. The tissues were homogenized using a SPEX Sample Prep Geno/Grinder 2010 for 5 minutes at 1500 RPM. 5μLs of 75mg/mL Ascorbic acid was added to the RIF standards and study samples before extraction to improve the autosampler stability of the extracts. The drugs and metabolites, corresponding labeled internal standards, MRM transitions and lower and upper limits of quantitation (LLOQ and ULOQ) are listed in Table S2. A list of drug and standard manufacturers is provided in Table S3.

## Tissue sectioning and matrix application

Twelve μm thick tissue sections were prepared using a Leica CM1850 cryostat (Buffalo Grove, IL) and thaw-mounted onto stainless steel slides (for MALDI mass spectrometry

imaging [MSI] analysis) or frosted glass microscope slides (for H&E staining). After sectioning, tissue sections were immediately transferred to a −80C freezer for storage.

Prior to MALDI-MSI analysis, tissue sections were removed from the −80°C freezer and allowed to reach room temperature for 15 minutes. For PZA, MXF and CFZ analysis, three mL of 50% methanol containing 2pmol/μL MXF-D3 (C/D/N Isotopes, Quebec, Canada) was applied to the surface by airspray deposition at 40psi, followed by 25mg/mL 2,5-Dihydroxybenzoic acid (Sigma-Aldrich, St Louis, MO) (50% methanol, 0.1% TFA). The airbrush (Paasche Model VL, Chicago, IL) was positioned at a distance of 30cm from the tissue and 30 passes over the tissue were performed with the tissue being allowed to dry for 30 seconds between coatings. For RIF analysis, three mL of 50% methanol containing 3pmol/μL RIF-D3 (TRC, Toronto) was applied to the surface by airspray deposition at 40psi, followed by 15mg/mL 2′,4′,6′-Trihydroxyacetophenone monohydrate (Acros Organics, Morris Plains, NJ) (50% methanol). The airbrush was positioned at a distance of 30cm from the tissue and 20 passes over the tissue were performed with the tissue being allowed to dry for 30 seconds between coatings. For Acetyl-INH, 5 mg/mL α-Cyano-4-hydroxycinnamic acid (Sigma-Aldrich, St Louis, MO) (50% ACN 0.1% TFA containing 2pmol/ μL INH-D4) was applied to the surface by airspray deposition at 40psi. The airbrush was positioned at a distance of 30cm from the tissue and 30 passes over the tissue were performed with the tissue being allowed to dry for 30 seconds between coatings.

## MALDI mass spectrometry imaging analysis

MALDI-MSI analysis was performed using a MALDI LTQ Orbitrap XL mass spectrometer (Thermo Fisher Scientific, Bremen, Germany) with a resolution of 60,000 at *m/z* 400, full width half maximum. The resolution was sufficient to resolve the drug and respective labeled standards peaks from background without the requirement for MS/MS and subsequent loss of signal. However, drug peak identities were confirmed by acquiring several MS/MS spectra directly from the dosed tissues.

Standards of PZA, MXF, acetyl-INH, RIF and desacetyl-RIF were analyzed both direct from the stainless steel target plate and spiked into control rat lung tissue to optimize instrument parameters. The limits of detection were determined as follows. Standards were spotted on drug-naïve tissue (3mm-diameter circles) and the weight of the underlying tissue (7.07$mm^2$) was estimated at 0.042mg, using the measured average weight of a 1×1.5cm×12μm section piece as 0.9mg. The limit of detection (LOD) was assessed from signals detected on spotted standards on granuloma and uninvolved lung sections following matrix application by airspray. The LOD were 1pmole or 3μg/g for PZA, 50 fmole or 200ng/g for MXF, 100fmol or 430ng/g for acetyl-INH, 50fmole or 410ng/g for RIF and desacetyl-RIF, and 50fmole or 240ng/g for CFZ.

For PZA, MXF, CFZ and acetyl-INH analysis, spectra were acquired in positive mode and with a mass window of *m/z* 100–500. This range covered the three small molecules, expected metabolites and any potential salt adduct peaks. A laser energy of 7.5μJ was applied and 50 laser shots were fired at each position (total of 1 microscan per position). The laser step size was set at 75–100μm (depending upon the size of the tissue section), at which small necrotic areas within lesions could easily be resolved and no overlapping of the laser

spot on adjacent acquisitions was observed. Images of the dehydrated cholesterol ion ([M $-H_2O+H]^+$ at *m/z* 369.351 derived from in-source fragmentation of cholesterol and cholesterol esters were generated from the same acquisitions. For RIF analysis, spectra were acquired in negative ion mode with a mass window of *m/z* 500–900. This range covered both RIF and its major metabolite desacetyl-RIF. A laser energy of 25μJ was applied and 35 laser shots were fired at each position (total of 1 microscan per position). The laser step size was set to 75μm.

Data visualization was performed using Thermo ImageQuest software. Normalized ion images of MXF were generated by dividing MXF $[M+H]^+$ signal (*m/z* 402.182 ± 0.003) by MXF-D3 $[M+H]^+$ signal (*m/z* 405.201 ± 0.003). Normalized ion images of PZA $[M+2H]^+$ (*m/z* 125.058 ± 0.003) were generated by normalizing to PZA-$^{15}$N-D3 [M+2H]+ (m/z 129.075 ± 0.003). Normalized ion images of RIF were generated by dividing RIF $[M-H]^-$ signal (*m/z* 821.397 ± 0.003) by RIF-D3 $[M-H]^-$ signal (*m/z* 824.416 ± 0.003). Normalized ion images of acetyl-INH and CFZ were generated by dividing acetyl-INH $[M+H]^+$ signal (*m/z* 180.077 ± 0.003) and CFZ $[M+H]^+$ signal (m/z 473.129 ± 0.003) by the total ion count (TIC). TIC normalization of acetyl-INH and CFZ images was validated by airspray deposition of 3 mL of 5pmol solution of Acetyl-INH or CFZ onto the tissue surface followed by 30 passes of 25 mg/mL DHB matrix. When either acetyl-INH $[M+H]^+$ or CFZ $[M+H]^+$ signal was normalized to the TIC, all tissue-derived ion suppression was compensated for, resulting in a homogenous signal across the tissue uninvolved lung, cellular and caseous tissue areas. Comparative TIC normalized images of acetyl-INH and CFZ versus raw images are shown in Figure S11.

For all drugs imaged, the signal responds linearly up to 1nmole/mL of internal standard, several orders of magnitude higher than levels achieved in tissues at therapeutic doses.

### Ion quantitation in regions of interest

Relative quantitation of drug levels within caseum and cellular lesion regions was performed using MSiReader[37]. The proprietary Thermo *RAW data format was converted to imzML using Raw to imzML converter to enable importation into MSiReader[38]. Regions of interest (ROIs) were drawn in each image covering either cellular lesion or caseum and the mean drug signal intensity within that region (normalized to the corresponding drug internal standard) was calculated following exportation of the ROI peak list into Excel.

### Lesion histology and cellularity of caseum

Sections (5μm thick) of each tissue block were cut, mounted on glass slides, and stained with hematoxylin and eosin[39]. Lesions were classified into non-necrotizing, cellular granulomas, necrotizing granulomas, and cavities. The cellularity of the necrotic material (or caseum) in large nodules and cavities was assessed by a reader masked to all data other than histology. Slides were read and caseum cellularity was scored from 1 to 4 using an adaption of the method of MacCarrick *et al*.[40] according to the estimated percentage of the lesion necrotic region with infiltrating leukocytes as follows: 1, 0 to 5%; 2, 6 to 20%; 3, 21 to 50% and 4, >50% (representative H&E stain images of each quartile are shown in Figure 2B).

### Drug accumulation assay in human THP-1 cells

Human macrophage-like THP-1 cell line (ATCC TIB-202) was maintained in RPMI 1640 medium (1× w/o L-glutamine, Corning cellgro 15-040-CV) supplemented with 10% fetal bovine serum and 2mM L-glutamine (Sigma G7513) at 37 °C in a 5% $CO_2$ incubator. THP-1 cells were initiated at a density of 2–4 × $10^5$ cells/mL in 75 $cm^2$ flasks. After 3 days of incubation, the number of viable cells were counted using the trypan blue exclusion protocol (http://www.lifetechnologies.com/us/en/home/references/gibco-cell-culture-basics/cell-culture-protocols/trypan-blue-exclusion.html) and diluted to 1 × $10^6$ cells/mL. Phorbol 12-myristate 13-acetate (PMA) was added to a final concentration of 100 nM, and 1 × $10^5$ cells were seeded into each well of 96-well tissue culture-treated plates (Greiner Bio One, 50-823-592). Plates were incubated overnight at 37 °C in a 5% $CO_2$ incubator to allow cells to attach to the bottom of the wells. After overnight incubation, cells were gently washed twice with equal volume of phosphate-buffered saline (PBS) to remove unattached and dead cells. To count and estimate the number of cells per well, cells were detached by incubation with 5 mM EDTA in phosphate buffered saline (PBS) for 20 minutes from a sub set of wells. Viable cells were counted using the trypan blue exclusion protocol.

To incubate cells with drugs, old media was removed carefully, and media with drugs were added. Cells were incubated at 37 °C for 30 minutes under ambient environment. After 30-minute incubation, media were removed carefully, and cells were gently washed twice with equal volume of ice cold PBS to remove any extracellular drug residuals. Cells were then lysed with equal volume of deionized water for 1 hour at 37 °C under ambient environment. Lysates were transferred to 1.5-mL centrifuge tubes and stored at −20 °C or analyzed right away.

Five anti-TB drugs were tested for accumulation in human THP-1 cells, INH (30μM, 40× MIC), PZA (4mM, 40× MIC), MXF (5μM, 4× MIC), RIF (4 μM, 4× MIC), CFZ (1μM, 4×MIC). When INH and PZA were first tested at 4× MIC concentrations, LC-MS signals were below the lowest limit of detection. Therefore, higher concentrations (40× MIC) were used in subsequent assays.

### Statistical analysis

A two-tailed z-test for proportions was used to compare the proportions of lesions that were above the minimum anaerobic bactericidal concentration for the study drugs. Two-tailed unpaired t-tests were used to analyze the correlation between moxifloxacin caseum/cellular concentration ratios and caseum cellularity scores. Statistical significance was concluded for *p* values below 0.05.

### Caseum binding assay

Specific pathogen-free, individually housed female New Zealand White (NZW) rabbits were used for aerosol infection by *M. tuberculosis* HN878 or *M. bovis* AF2122, as previously described[12,41]. Briefly, rabbits were exposed to *M. tuberculosis*- or *M. bovis*-containing aerosol using a nose-only delivery system. Three hours post-infection, three rabbits were euthanized, and serial dilutions of the lung homogenates were cultured on Middlebrook 7H11 agar plates to enumerate the number of bacterial colony forming units (CFUs)

implanted in the lungs. The infection was allowed to progress for 4 weeks (*M. bovis*) or 12 to 16 weeks (*M. tuberculosis*) prior to necropsy and collection of cavity caseum. All animal studies were carried out in accordance with the Guide for the Care and Use of Laboratory Animals of the National Institutes of Health, with approval from the Institutional Animal Care and Use Committee of the New Jersey Medical School, Newark, NJ, and the National Institute of Allergy and Infectious Diseases (National Institutes of Health), Bethesda, MD.

The RED device comprises two side-by-side chambers separated by a vertical cylinder of dialysis membrane (Molecular weight cut-off = ~8000)[42]. Caseum samples were diluted 10-fold in PBS and homogenized. Drug stock solutions were added to the homogenized samples to give the final concentration of 5μM (<1% DMSO). The inserts are placed in the open wells of the Teflon base plate. 200μl of spiked plasma was placed in the sample chambers and the buffer chambers were filled with 350μl of PBS. The plates are sealed and incubated at 37°C for 4hrs on an orbital shaker set at 200rpm. Following incubation, 50μl of plasma from the sample chamber was transferred to tube containing 50μl of neat PBS. Similarly, 50μl of PBS was transferred from the buffer chamber to a tube containing 50μl of neat plasma. 400μl of an organic solvent mixture (30/70 methanol/ACN with internal standard) was added to each sample. Samples were vigorously vortexed and centrifuged. The supernatant was transferred to 96-well plates and stored at −20°C.

Fraction unbound ($f_u$) in undiluted caseum was calculated using Equation 1, where the dilution factor (D) is equals to 10. Recovery (mass balance) for each assay was calculated using Equation 2.

$$\text{Undiluted} f_u = \frac{1/D}{\left(\left(\frac{1}{fu}\right) - 1\right) + 1/D} \quad (1)$$

$$\text{Recovery} = \frac{mass\ in\ sample\ chamber + mass\ in\ buffer\ chamber}{mass\ in\ sample\ chamber\ att=0} \times 100\% \quad (2)$$

## Supplementary Material

Refer to Web version on PubMed Central for supplementary material.

## Acknowledgments

We thank D. Young and the funders of the Grand Challenge for Global Health (GCGH 11) consortium, for their faith and support. We are grateful to the subjects who enrolled in the study, Y. Kim and M.S. Kong, Y. Cai, J. Gonzales and L. Goldfeder and the clinical teams at the three Korean centers for their efforts in making the study a success. We thank S. Dorman, D. Alland and H. Boshoff for sharing clinical MIC and *in vitro* MAC datasets, M. Stoeckli and D. Staab for providing access to the MALDI imaging platform at the Novartis Institutes for Biomedical Research (Basel, CH), E. Eugenin, J. Flynn and J. Mattila for sharing images of *M. tuberculosis* in non-human primate lesions, and T Dick for many stimulating discussions and advice with the manuscript. This work was carried out with funding from National Institutes of Health grant 1R01AI106398-01 (V.D.), grant OPP1066499 (V.D.) from the Bill and Melinda Gates Foundation, the Intramural Research Program of the National Institute of Allergy and Infectious Diseases, National Institutes of Health (C.E.B.) and the National Heart, Lung and Blood Institute (K.N.O.), as well as funding from the Korean Centers for Disease Control of the Korean Ministry of Health and Welfare to the International Tuberculosis Research Center.

## REFERENCES


1. Hoff DR, et al. Location of intra- and extracellular M. tuberculosis populations in lungs of mice and guinea pigs during disease progression and after drug treatment. PloS one. 2011; 6:e17550. [PubMed: 21445321]
2. Li SY, et al. Evaluation of Moxifloxacin-Containing Regimens in Pathologically Distinct Murine Tuberculosis Models. Antimicrobial agents and chemotherapy. 2015; 59:4026–4030. [PubMed: 25918146]
3. Fox W, Ellard GA, Mitchison DA. Studies on the treatment of tuberculosis undertaken by the British Medical Research Council tuberculosis units, 1946–1986, with relevant subsequent publications. The international journal of tuberculosis and lung disease : the official journal of the International Union against Tuberculosis and Lung Disease. 1999; 3:S231–S279.
4. Mitchison DA. The action of antituberculosis drugs in short-course chemotherapy. Tubercle. 1985; 66:219–225. [PubMed: 3931319]
5. Lenaerts AJ, et al. Location of persisting mycobacteria in a Guinea pig model of tuberculosis revealed by r207910. Antimicrobial agents and chemotherapy. 2007; 51:3338–3345. [PubMed: 17517834]
6. Lakshminarayana SB, et al. Comprehensive physicochemical, pharmacokinetic and activity profiling of anti-TB agents. The Journal of antimicrobial chemotherapy. 2015; 70:857–867. [PubMed: 25587994]
7. Nuermberger EL, et al. Moxifloxacin-containing regimen greatly reduces time to culture conversion in murine tuberculosis. Am J Respir Crit Care Med. 2004; 169:421–426. Epub 2003 Oct 2024. [PubMed: 14578218]
8. Gillespie SH, et al. Four-month moxifloxacin-based regimens for drug-sensitive tuberculosis. The New England journal of medicine. 2014; 371:1577–1587. [PubMed: 25196020]
9. Jindani A, et al. High-dose rifapentine with moxifloxacin for pulmonary tuberculosis. The New England journal of medicine. 2014; 371:1599–1608. [PubMed: 25337749]
10. Dartois V. The path of anti-tuberculosis drugs: from blood to lesions to mycobacterial cells. Nature reviews. Microbiology. 2014; 12:159–167. [PubMed: 24487820]
11. Via LE, et al. Host-Mediated Bioactivation of Pyrazinamide: Implications for Efficacy, Resistance, and Therapeutic Alternatives. ACS Infect Dis. 2015; 1:203–214. [PubMed: 26086040]
12. Via LE, et al. Tuberculous Granulomas are Hypoxic in Guinea pigs, Rabbits, and Non-Human Primates. Infect Immun. 2008; 76:2333–2340. [PubMed: 18347040]
13. Zhang Y, Scorpio A, Nikaido H, Sun Z. Role of acid pH and deficient efflux of pyrazinoic acid in unique susceptibility of Mycobacterium tuberculosis to pyrazinamide. J Bacteriol. 1999; 181:2044–2049. [PubMed: 10094680]
14. Canetti, G. The Tubercle Bacillus. Springer Publishing COmpany; 1955.
15. Aber VR, Nunn AJ. [Short term chemotherapy of tuberculosis. Factors affecting relapse following short term chemotherapy]. Bull Int Union Tuberc. 1978; 53:276–280. [PubMed: 387141]
16. Chang KC, Leung CC, Yew WW, Ho SC, Tam CM. A nested case-control study on treatment-related risk factors for early relapse of tuberculosis. American journal of respiratory and critical care medicine. 2004; 170:1124–1130. [PubMed: 15374844]
17. Prideaux B, Stoeckli M. Mass spectrometry imaging for drug distribution studies. J Prot. 2012; 75:4999–5013.
18. Reyzer ML, Caprioli RM. MALDI-MS-based imaging of small molecules and proteins in tissues. Current opinion in chemical biology. 2007; 11:29–35. [PubMed: 17185024]
19. Tischler AD, McKinney JD. Contrasting persistence strategies in Salmonella and Mycobacterium. Current opinion in microbiology. 2010; 13:93–99. [PubMed: 20056478]
20. Michot JM, Seral C, Van Bambeke F, Mingeot-Leclercq MP, Tulkens PM. Influence of efflux transporters on the accumulation and efflux of four quinolones (ciprofloxacin, levofloxacin, garenoxacin, and moxifloxacin) in J774 macrophages. Antimicrobial agents and chemotherapy. 2005; 49:2429–2437. [PubMed: 15917543]

21. Kjellsson MC, et al. Pharmacokinetic evaluation of the penetration of antituberculosis agents in rabbit pulmonary lesions. Antimicrobial agents and chemotherapy. 2012; 56:446–457. [PubMed: 21986820]
22. Prideaux B, et al. High-sensitivity MALDI-MRM-MS imaging of moxifloxacin distribution in tuberculosis-infected rabbit lungs and granulomatous lesions. Anal Chem. 2011; 83:2112–2118. [PubMed: 21332183]
23. Irwin SM, et al. Limited activity of clofazimine as a single drug in a mouse model of tuberculosis exhibiting caseous necrotic granulomas. Antimicrobial agents and chemotherapy. 2014; 58:4026–4034. [PubMed: 24798275]
24. Pichugin AV, Yan BS, Sloutsky A, Kobzik L, Kramnik I. Dominant role of the sst1 locus in pathogenesis of necrotizing lung granulomas during chronic tuberculosis infection and reactivation in genetically resistant hosts. Am J Pathol. 2009; 174:2190–2201. [PubMed: 19443700]
25. Kell DB, Oliver SG. How drugs get into cells: tested and testable predictions to help discriminate between transporter-mediated uptake and lipoidal bilayer diffusion. Front Pharmacol. 2014; 5:231. [PubMed: 25400580]
26. Baik J, Rosania GR. Macrophages sequester clofazimine in an intracellular liquid crystal-like supramolecular organization. PloS one. 2012; 7:e47494. [PubMed: 23071814]
27. Nathan C, Barry CE 3rd. TB drug development: immunology at the table. Immunol Rev. 2015; 264:308–318. [PubMed: 25703568]
28. Rastogi N, et al. Emergence during unsuccessful chemotherapy of multiple drug resistance in a strain of Mycobacterium tuberculosis. European journal of clinical microbiology & infectious diseases : official publication of the European Society of Clinical Microbiology. 1992; 11:901–907.
29. Calver AD, et al. Emergence of increased resistance and extensively drug-resistant tuberculosis despite treatment adherence, South Africa. Emerging infectious diseases. 2010; 16:264–271. [PubMed: 20113557]
30. Merker M, et al. Whole genome sequencing reveals complex evolution patterns of multidrug-resistant Mycobacterium tuberculosis Beijing strains in patients. PloS one. 2013; 8:e82551. [PubMed: 24324807]
31. Sun G, et al. Dynamic population changes in Mycobacterium tuberculosis during acquisition and fixation of drug resistance in patients. J Infect Dis. 2012; 206:1724–1733. [PubMed: 22984115]

## REFERENCES

32. Lee J, et al. Sensititre MYCOTB MIC plate for testing Mycobacterium tuberculosis susceptibility to first- and second-line drugs. Antimicrobial agents and chemotherapy. 2014; 58:11–18. [PubMed: 24100497]
33. O'Connell ML, et al. Lung manifestations in an autopsy-based series of pulmonary or disseminated nontuberculous mycobacterial disease. Chest. 2012; 141:1203–1209. [PubMed: 22194586]
34. Okumura M, et al. Clinical factors on cavitary and nodular bronchiectatic types in pulmonary Mycobacterium avium complex disease. Internal medicine. 2008; 47:1465–1472. [PubMed: 18703856]
35. Yuan MK, et al. Comparative chest computed tomography findings of non-tuberculous mycobacterial lung diseases and pulmonary tuberculosis in patients with acid fast bacilli smear-positive sputum. BMC pulmonary medicine. 2014; 14:65. [PubMed: 24755048]
36. Wagner C, Sauermann R, Joukhadar C. Principles of antibiotic penetration into abscess fluid. Pharmacology. 2006; 78:1–10. [PubMed: 16864973]
37. Robichaud G, Garrard KP, Barry JA, Muddiman DC. MSiReader: an open-source interface to view and analyze high resolving power MS imaging files on Matlab platform. Journal of the American Society for Mass Spectrometry. 2013; 24:718–721. [PubMed: 23536269]
38. Schramm T, et al. imzML--a common data format for the flexible exchange and processing of mass spectrometry imaging data. J Proteomics. 2012; 75:5106–5110. [PubMed: 22842151]
39. Via LE, et al. Infection Dynamics and Response to Chemotherapy in a Rabbit Model of Tuberculosis using [18F]2-Fluoro-Deoxy-D-Glucose Positron Emission Tomography and

Computed Tomography. Antimicrobial agents and chemotherapy. 2012; 56:4391–4402. [PubMed: 22687508]

40. MacCarrick MJ, et al. Does hypercapnia ameliorate hyperoxia-induced lung injury in neonatal rats? Lung. 2010; 188:235–240. [PubMed: 20033196]
41. Subbian S, et al. Chronic pulmonary cavitary tuberculosis in rabbits: a failed host immune response. Open Biol. 2011; 1
42. Waters NJ, Jones R, Williams G, Sohal B. Validation of a rapid equilibrium dialysis approach for the measurement of plasma protein binding. Journal of pharmaceutical sciences. 2008; 97:4586–4595. [PubMed: 18300299]

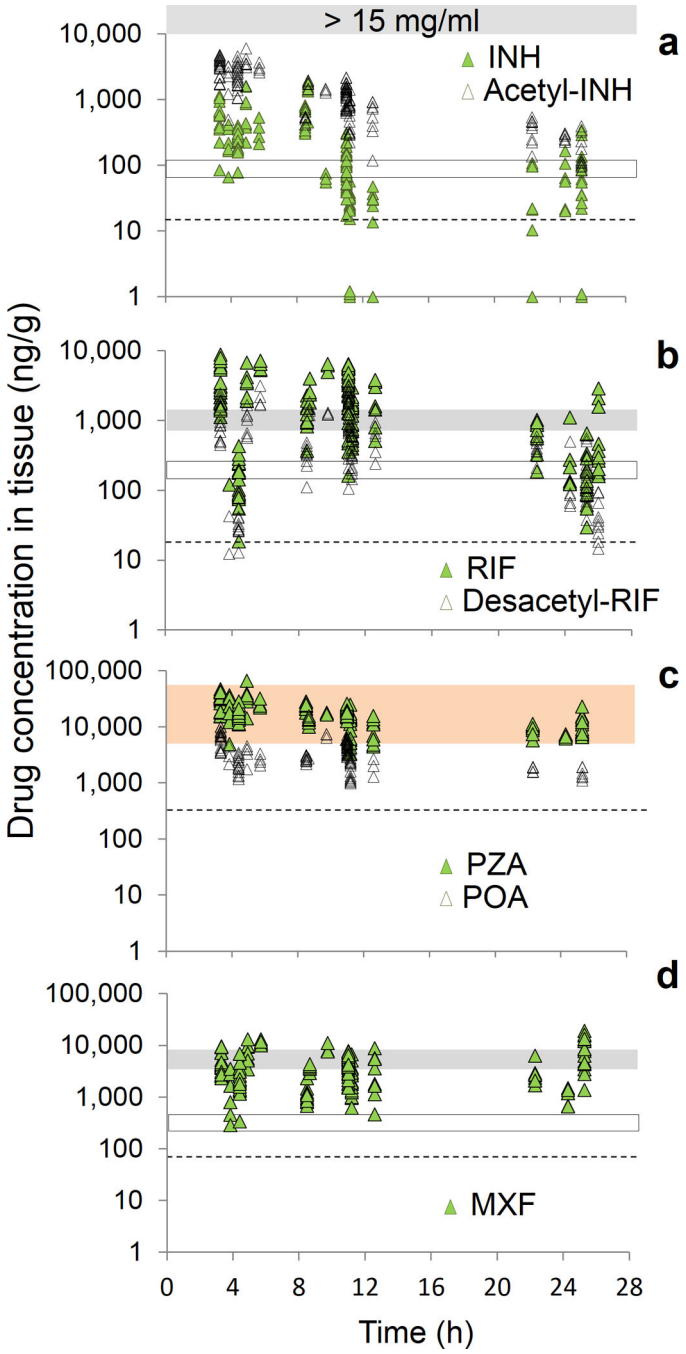


**Figure 1.**

Quantitative drug distribution in human pulmonary lesions. Closed nodules, cavity wall and cavity caseum samples from each subject were homogenized prior to measuring the concentrations of INH (**a**), RIF (**b**), PZA (**c**), and MXF (**d**). Each subject contributed an average of 11 to 12 lesions. The major metabolites of INH (acetyl-INH), RIF (desacetyl-RIF) and PZA (POA) are shown as black empty symbols in **a,b,c**. Note that INH is a prodrug activated by *M. tuberculosis*' catalase, the product of which forms transient NAD adducts that may display a distinct distribution pattern but cannot be captured by LCMS or

MALDI imaging. The dotted line indicates the lower limit of quantitation. The clear and grey shaded boxes (**a,b,d**) represent clinical MIC[32] and MAC[6] ranges, respectively. The orange shaded box in **c** is the range of PZA activity in acidic conditions[13].

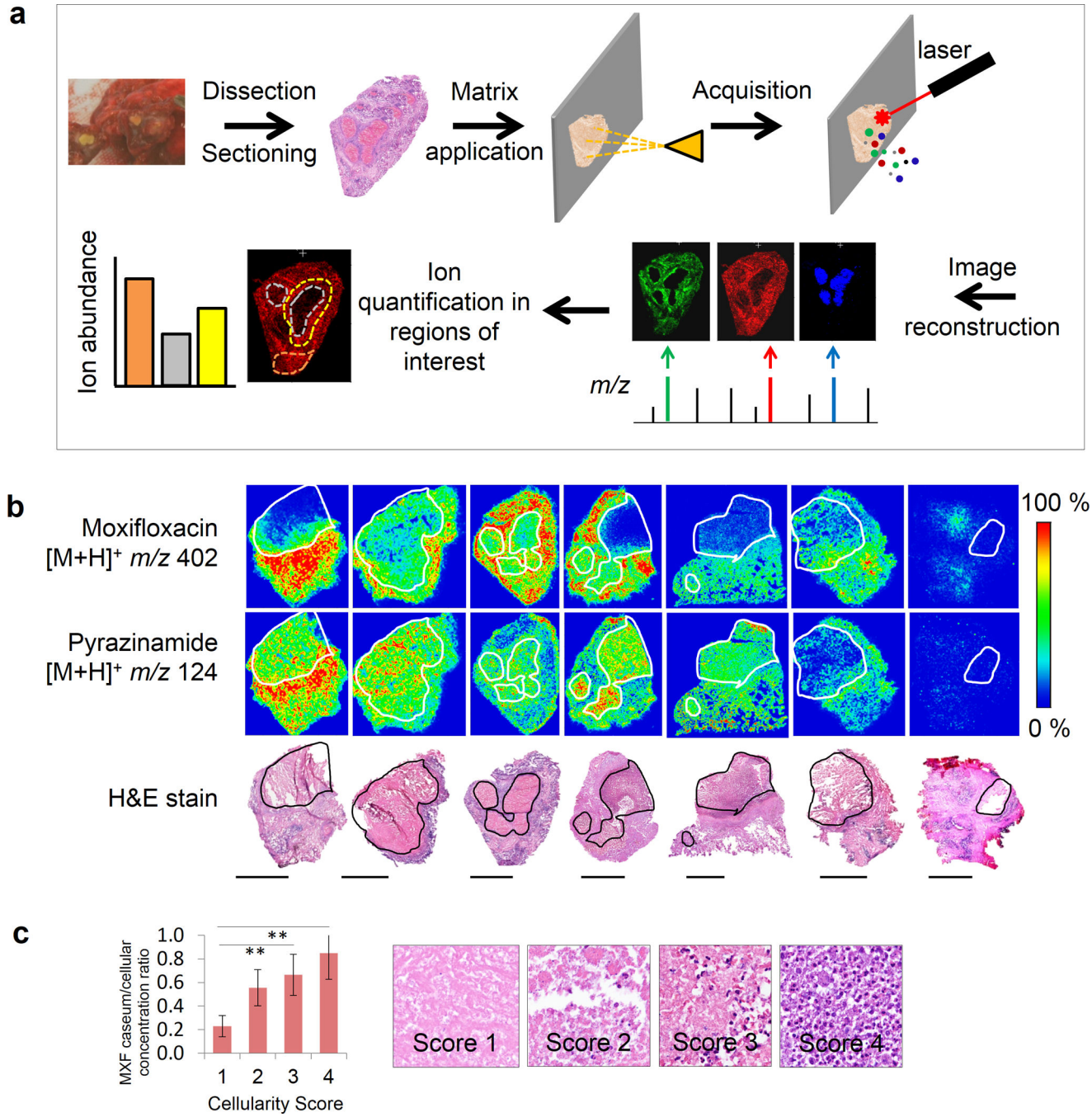


**Figure 2.**

Two-dimensional imaging of MXF and PZA by MALDI mass spectrometry. (**a**) Schematic of MALDI mass spectrometry imaging of small molecules in TB infected lung tissue, from tissue sectioning to data acquisition and overlay with histology stain of an adjacent tissue section. The relative ion abundance of specific analytes in regions of interest delineated based on histology staining can be measured to provide semi-quantitative data. (**b**)Ion maps of PZA and MXF in representative lung lesions sampled throughout the dosing interval; the signal intensity is fixed for each drug and indicated by the rainbow color scale bar to the

right. Hematoxylin and Eosin (H&E) staining of adjacent sections is shown below the ion maps. Black/white contour lines highlight the necrotic center of each lesion. Asterisks indicate lesions from patients at steady state for $MXF^{(*)}$ or $PZA^{(**)}$. Black scale bar: 5mm. (**c**) Diffusion of MXF in caseum as a function of caseum cellularity. Two-tailed unpaired t-tests were used to analyze the correlation between moxifloxacin caseum/cellular concentration ratios and caseum cellularity scores. Means +/− s.d. are shown (n=3). ** $p < 0.05$. A typical H&E example representative of each cellularity score is shown on the right.

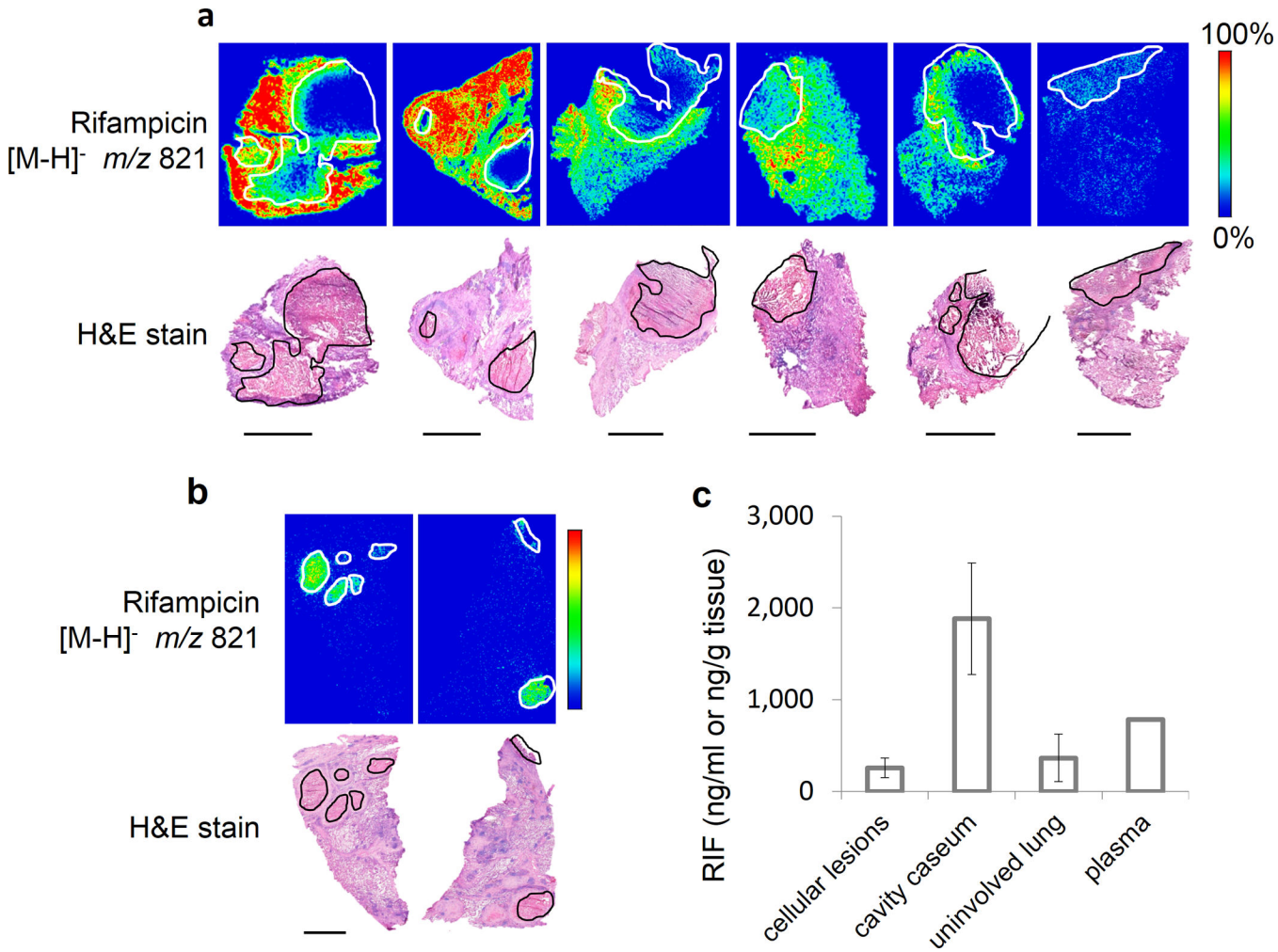


**Figure 3.**

Penetration of RIF in TB lesions. (**a**) Ion maps of RIF in lung lesions collected following a single drug dose; (**b**) RIF accumulates in necrotic foci at steady-state. H&E staining of adjacent sections are shown below each set of ion maps. Black/white contour lines highlight the necrotic center of each lesion. Black scale bar: 5mm. (**c**) Average RIF concentration in plasma, uninvolved lung tissue, and lesions in one subject at steady state. The samples were collected 26h after the last of 180 RIF doses was administered. Means +/− s.d. of 3 to 5 lung pieces or distinct lesions are shown.

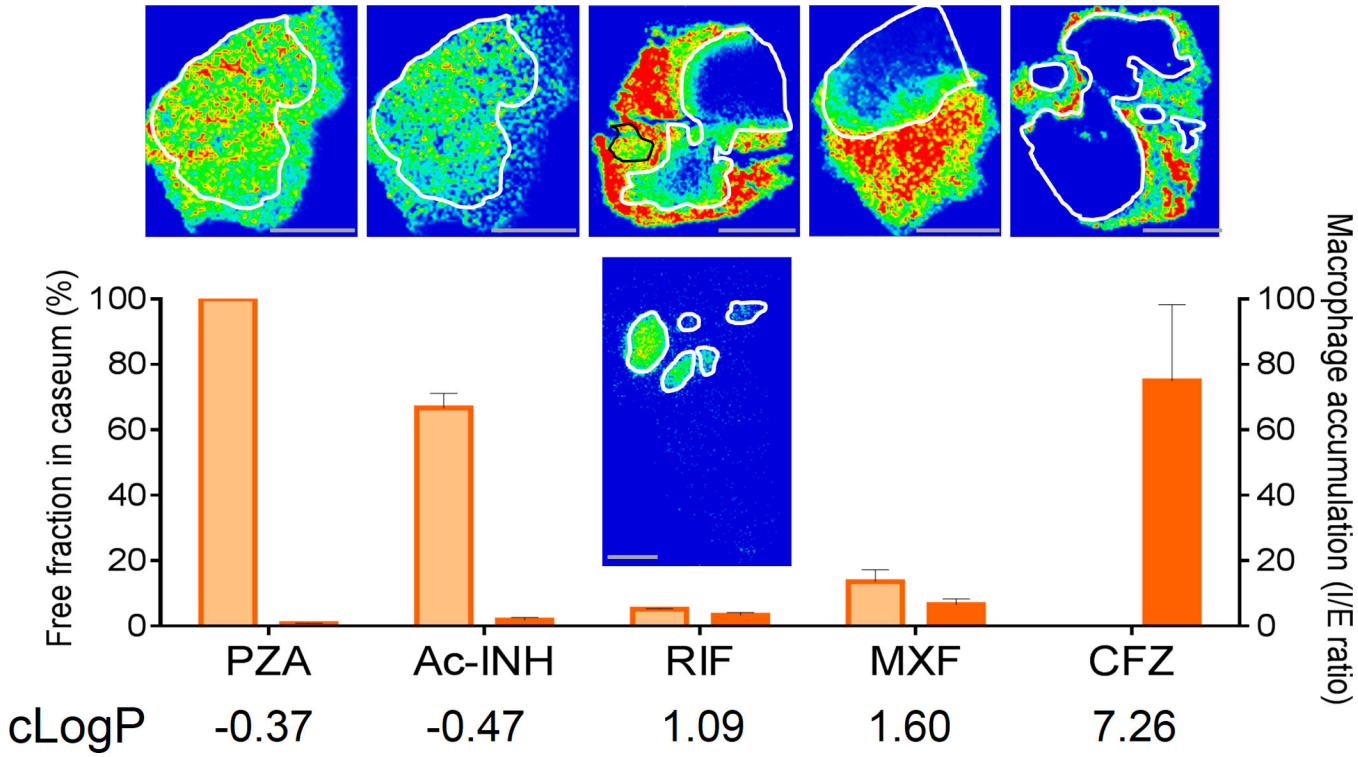


**Figure 4.**

Factors affecting drug diffusion into caseum. Relationship between caseum binding (orange bars), accumulation into macrophages (red bars), lipophilicity (cLogP) and diffusion into caseum *in vivo* for the study drugs. Each assay was performed in triplicates, with means +/− s.d. shown. Scale bar: 5mm